2904 *Chem. Mater.* **2009,** *21,* 2904–2911
DOI:10.1021/cm900645c

CHEMISTRY OF MATERIALS
Article

Structural Characterization of Interlayer Expanded Zeolite Prepared From Ferrierite Lamellar Precursor

Juanfang Ruan,*,† Peng Wu,‡ Ben Slater,§ Zhonglin Zhao,‡ Leilei Wu,‡ and Osamu Terasaki†

†*Division of Structural Chemistry, Arrhenius Laboratory, Stockholm University, S-10691, Stockholm, Sweden,* ‡*Shanghai Key Laboratory of Green Chemistry and Chemical Processes, Department of Chemistry, East China Normal University, North Zhongshan Road 3, Shanghai 200062, P. R. China, and* §*Department of Chemistry, University College London, 20 Gordon Street, London WC1H 0AJ United Kingdom*

Received March 6, 2009. Revised Manuscript Received April 17, 2009

A novel methodology was successfully developed to expand the structure of zeolitic lamellar precursors through molecular alkoxysilylation. The method has been applied to PREFER (lamellar precursor of ferrierite). As a result, a novel crystalline interlayer expanded zeolite named as IEZ-FER (IEZ is the abbreviation of interlayer expanded zeolite) with enlarged distance perpendicular to the layer was synthesized through interlayer molecular alkoxysilylation. In this paper, the structure of IEZ-FER has been comprehensively studied by various means such as electron diffraction, high-resolution electron microscopy (HREM) and structure modeling. Our studies provide evidence that IEZ-FER preserves the pentasil layers corresponding to that found in the known three-dimensional (3D) FER zeolite, but it also shows a distinct expansion of the layer spacing (~5 Å). The newly formed channel system is distinct from that of the known 3D FER structure,which has 8-membered ring (MR) and 10MR pores along the [010] and [001] directions, respectively; IEZ-FER exhibits 10MR and 12MR pores along the [010] and [001] directions, respectively, in the interlayer space, which can be shown to explain the expansion in between layers. Furthermore, the formation of the large pores could be realized by the insertion of monolayer of Si species between the layers, and it explains the unique interlayer cross-linkages ($Si(OH)(SiO_2)_3$ and $Si(OH)_2(SiO_2)_2$) present in the interlayer.

Introduction

Zeolites are widely used as catalysts, ion exchangers, detergents, and adsorbents, and their range of applications still continues to grow.[1] Therefore, there is always a large demand for new types of zeolites with high surface areas and thermal stability as well as special physicochemical properties. Because of this, the synthesis of new zeolites has had a very successful period during past decades. In particular, the discovery of new zeolitic structures formed from zeolitic layered precursors of silicates or aluminosilicates has made a major contribution to the extension of the existing zeolite family,[2−12] because conventional zeolite structures provide little possibility for structural modification once they are synthesized. Layered silicate precursors are composed of rigid lamellae, which are linked to each other by weak bonds. These bonds can often be cleaved, which allows flexibility in the third dimension with regard to interlayer distance and spatial arrangements of the layers. In this respect, the interlayer space of layered silicate precursors can be variously modified by many approaches, such as pillaring, delamination, intercalation, and silylation, to produce a number of new zeolite-type materials to meet specific needs in catalytic and separation processes. One notable example is MCM-22 with the MWW topology, the precursor of which has 2D layered structure, and the 3D network is formed upon calcinations through the condensation of the silanol groups located on the layer surface.[2] New materials such as MCM-36[13] and ITQ-2 [14] were obtained by pillaring and delaminating the swollen MCM-22 precursor, respectively. In addition, a material named Ti-YNU-1 was obtained occasionally when Ti-containing MWW lamellar precursor was treated in

*Corresponding author. Fax: 46-46-2224413. Tel: 46-46-2224812. E-mail: juanfang.ruan@fkem1.lu.se.

(1) Davis, M. E. *Nature* **2002**, *417*, 813.
(2) Leonowicz, M. E.; Lawton, J. A.; Lawton, S. L.; Rubin, M. K. *Science* **1994**, *264*, 1910.
(3) Schreyeck, L.; Caullet, P.; Mougenel, J. C.; Guth, J. L.; Marler, B. *Microporous Mater.* **1996**, *6*, 259.
(4) Blake, A. J.; Franklin, K. R.; Lowe, B. M. *J. Chem. Soc., Dalton Trans.* **1998**, 2513.
(5) Ikeda, T.; Akiyama, Y.; Oumi, Y.; Kawai, A.; Mizukami, F. *Angew. Chem., Int. Ed.* **2004**, *43*, 4892.
(6) Zanardi, S.; Alberti, A.; Cruciani, G.; Corma, A.; Fornés, V.; Brunelli, M. *Angew. Chem., Int. Ed.* **2004**, *43*, 4933.
(7) Marler, B.; Ströter, N.; Gies, H. *Microporous Mesoporous Mater.* **2005**, *83*, 201.
(8) Wang, Y. X.; Gies, H.; Marler, B.; Müller, U. *Chem. Mater.* **2005**, *17*, 43.
(9) Mochizuki, D.; Shimojima, A.; Imagawa, T.; Kuroda, K. *J. Am. Chem. Soc.* **2005**, *127*, 7183.
(10) Wang, Y. X.; Gies, H.; Lin, J. H. *Chem. Mater.* **2007**, *19*, 4184.
(11) Choi, S.; Coronas, J.; Jordan, E.; Oh, W.; Nair, S.; Onorato, F.; Shantz, D. F.; Tsapatsis, M. *Angew. Chem., Int. Ed.* **2008**, *47*, 552.
(12) Li, Z. F.; Marler, B.; Gies, H. *Chem. Mater.* **2009**, *20*, 1896.
(13) Roth, W. J.; Kresge, C. T.; Vartuli, J. C.; Leonowicz, M. E.; Fung, A. S.; McCullen, S. B. *Stud. Surf. Sci. Catal.* **1995**, *94*, 301.
(14) Corma, A.; Fornés, V.; Pergher, S. B.; Maesen, Th. L. M.; Buglass, J. G. *Nature* **1998**, *396*, 353.

 Published on Web 05/19/2009

aqueous acid solution.[15] The investigations into the structure of this material suggested that it was probably formed through the pillaring of the Si species between the layers, which leads to the formation of 12-membered ring (MR) in the interlayer space.[16] Therefore, the pillaring of layered materials by intercalation with suitable molecules in the interlayer space, can lead to ordered pore structures. Also, following this approach, it is possible to tune the interlayer pore size/shape and chemical functionality by choosing suitable intercalating species. The order of the interlayer structure fully depends on the extent and degree of the pillaring. At present, it is still a major challenge for scientific researchers to postsynthesize well-ordered expanded structure through the pillaring process from lamellar precursors.

It was reported that a novel crystalline layered silicate could be synthesized by the alkoxysilylation of layered silicate octosilicate with dialkoxydichlorosilanes and the subsequent reaction within the interlayers.[17] Recently, we proposed a method based on molecular alkoxysilylation of lamellar precursors for constructing new 3D zeolitic structures with expanded pore windows.[18] Scheme 1 shows the schematic drawing of constructing a new interlayer expanded structure (IEZ) compared to the directly calcined structure (3D) by inserting diethoxydimethylsilane ($Me_2Si(OEt)_2$) species into lamellar precursors through dialkoxysilylation. The method has first been employed to MWW precursors, then extended to FER and CDO lamellar precursors. Novel crystalline interlayer expanded zeolites denoted IEZ-ABC (ABC: MWW, FER, and CDO) with enlarged pores have been synthesized. True structures of these interlayer expanded zeolites remain unresolved up to date. Here, we report on the structure elucidation of IEZ-FER in detail mainly by transmission electron microscopy (TEM) in combination with other characterization methods.

Experimental Section

Synthesis. FER lamellar precursor, so-called PREFER, was hydrothermally synthesized using 4-amino-2,2,6,6-tetramethylpiperidine as a structure-directing agent following a previously reported method.[3] The gel with the composition of 1.0:1.0:1.5:1.0:15 SiO_2:SDA:NH_4F:HF:H_2O was crystallized at 170 °C for 7 days. PREFER was then alkoxysilylated with diethoxydimethylsilane ($Me_2Si(OEt)_2$) species under low pH conditions. Typically, 1 g of precursor was mixed with 50 g of aqueous solution of 2 M HNO_3 and a desirable amount of $Me_2Si(OEt)_2$. The mixture was then tumbled in a Teflon-lined autoclave at 150 °C for 20 h to induce the silylation. The silylated samples were filtered and washed with deionized water repeatedly and dried at 120 °C for 10 h. The samples were further

Scheme 1. Alkoxysilylation of Lamellar Precursor by Diethoxydimethylsilane and Calcination of the Silylated Product or Lamellar Precursor

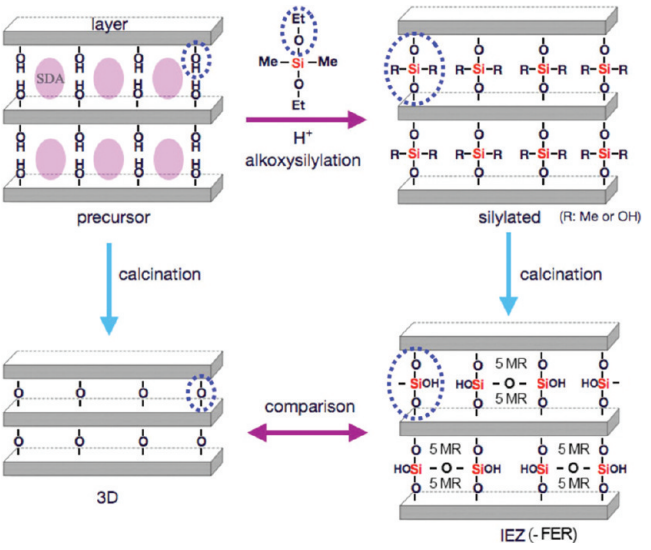

calcined in air at 550 °C for 10 h to remove any organic species. The resulting interlayer expanded zeolite is denoted IEZ-FER. On the other hand, PREFER was directly calcined in air at 550 °C for 10 h to obtain 3D FER.

Characterizations. Powder X-ray diffraction (XRD) patterns were collected on a MAC Science MX-Labo diffractiometer using monochromatic Cu $K\alpha_1$ radiation and Si as an internal standard. Crystal size and morphology was examined by scanning electron microscopy on a Hitachi S-4800 microscope without metal coating. Transmission electron microscopy measurements were carried out at 300 kV with a JEOL 3010 electron microscope (Cs = 0.6 mm, point resolution 1.7 Å) equipped with Leaser TV rate camera and Gatan CCD camera. Samples for TEM observations were crushed in an agate mortar for *ca.* 10 min, dispersed in ethanol (95 vol %) by ultrasonicating, and then dropped onto a carbon microgrid. Selected area electron diffraction (SAED) patterns and high-resolution electron microscopy (HREM) images were recorded on Kodak SO-163 electron microscope film using low-electron-dose conditions. HREM image simulations were carried out through the multislice method using the MacTempas program as a function of crystal thickness and defocus value under the parameters of an accelerated voltage = 300 kV, Cs = 0.6 mm, semiangle of beam convergence = 0.6 mrad, g value = 2 $Å^{-1}$. Fourier filtered images were obtained using Gatan DigitalMicrograph program by the inverse Fourier transform of the Bragg peaks on Fourier diffractograms (FDs) or the Bragg peaks with diffuse streaks on FDs. Ar adsorption isotherms were measured on a BELSORP 28SCA instrument. ^{29}Si MAS NMR spectra were recorded on a JEOL JNM ECA-400 multinuclear solid-state magnetic resonance spectrometer.

To analyze the conformational arrangement of the pillared Si atoms, we performed calculations using a two-tier scheme to reduce the computational expense of the study: first, hypothecated unit cells were relaxed using the GULP program,[19] employing the recently developed forcefield due to Ugliengo et al.[20] In the second stage, the relaxed cell and coordinates were used as the starting geometry for a DFT plane wave geometry

(15) Fan, W. B.; Wu, P.; Namba, S.; Tatsumi, T. *Angew. Chem., Int. Ed.* **2004**, *43*, 236.
(16) Ruan, J. F.; Wu, P.; Slater, B.; Terasaki, O. *Angew. Chem., Int. Ed.* **2005**, *44*, 6719.
(17) Mochizuki, D.; Shimojima, A.; Kuroda, K. *J. Am. Chem. Soc.* **2002**, *124*, 12082.
(18) Wu, P.; Ruan, J. F.; Wang, L. L.; Wu, L. L.; Wang, Y.; Liu, Y. M.; Fan, W. B.; He, M. Y.; Terasaki, O.; Tatsumi, T. *J. Am. Chem. Soc.* **2008**, *130*, 8178.
(19) Gale, J. D.; Rohl, A. L. *Mol. Simul.* **2003**, *29*, 291.
(20) Pedone, A.; Malavasi, G.; Menziani, M. C.; Segre, U.; Musso, F.; Corno, M.; Civalleri, B.; Ugliengo, P. *Chem. Mater.* **2008**, *20*, 2522.

optimization study using the program CASTEP.[21] In the latter study, a k-point sampling grid of 1 × 1 × 2 was used and the kinetic energy cutoff was 340 eV. Ultrasoft pseudpotentials were used with the PBE functional.

Results and Discussion

Figure 1 shows powder XRD patterns of calcined 3D FER, silylated IEZ-FER, calcined IEZ-FER and the precursor of ferrierite (PREFER). All XRD patterns show characteristic peaks of the FER-type framework structure. Upon calcination of PREFER, the adjacent 2D layers link into the 3D FER structure with interlayer windows of 8MR and10MR pores (along [010] and [001] directions) through the condensation of the silanol groups on the layer surface. As a result of structural condensation occurred perpendicular to the layers along *a* axis, the diffraction peaks related to *a* axis for 3D FER shift to high scattering angle. However, for IEZ-FER, the diffraction peaks associated with the *a* axis shift to a lower scattering angle in comparison with 3D FER because of the silylation with $Me_2Si(OEt)_2$ species, which implies that the insertion of $Me_2Si(OEt)_2$ species leads to the expansion of the interlayer space. Table 1 lists unit-cell parameters of FER obtained from the powder XRD data. The calculated *a* parameter of calcined IEZ-FER is enlarged by ca. 4.97 Å compared with that of 3D FER, but *b* and *c* parameters remain almost constant because of the rigid pentasil layered structure. These observations apparently suggest that the postprocessing, like silylation and further calcination, still preserves the intralayer structure, but alters the interlayer structure. Although the interlayer structure is expanded in IEZ-FER, SEM images in Figure 2 still clearly show that IEZ-FER possesses similar platelike morphology as 3D FER. No any significant changes in crystal thickness and size were observed.

To further confirm the integrity of the intralayer structure and the expansion of the interlayer structure observed from XRD, we show in Figure 3 selected area electron diffraction (SAED) patterns of calcined 3D FER (a−d) and IEZ-FER (e−h) taken along the [100], [010], [001], and [0$\bar{1}$1] directions using the same microscopy condition. The SAED pattern of IEZ-FER along the [100] zone axis (Figure 3e) is identical to the SAED pattern of 3D FER (Figre 3a), which strongly demonstrated that the intralayer structure remains intact. Moreover, the SAED patterns of IEZ-FER along the [010], [001], and [0$\bar{1}$1] zone axes (Figure 3f−h) are almost identical to the SAED patterns of 3D FER (Figure 3b−d) from the view of the symmetry and intensity except for the distinct decreasing *a**, which also indicate that IEZ-FER possesses the layered structure of FER topology, but the interlayer space was expanded (*a** decreased and *a* increased) because of the insertion of the $Me_2Si(OEt)_2$ species. Unit-cell parameters calculated from the SAED patterns are given in Table 1 as well. We found that

(21) Clark, S. J.; Segall, M. D.; Pickard, C. J.; Hasnip, P. J.; Probert, M. J.; Refson, K.; Payne, M. C. *Z. Krystallogr.* **2005**, *220*, 567.

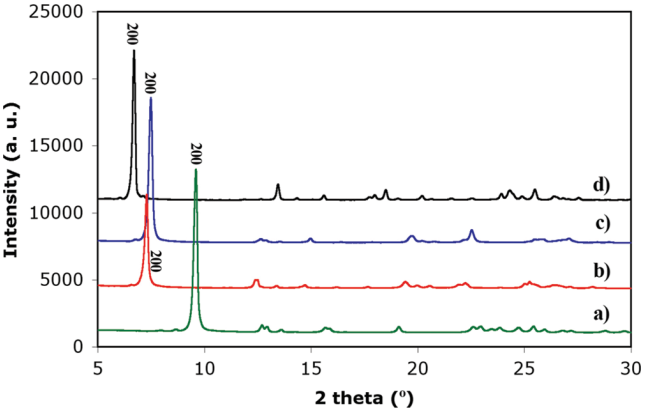

Figure 1. XRD patterns of (a) calcined 3D FER, (b) silylated IEZ-FER, (c) calcined IEZ-FER, and (d) PREFER.

Table 1. Unit-Cell Parameters

	unit-cell parameters	
	XRD[a]	ED[b]
3D FER (calcined)	a = 18.7719(5) Å b = 14.0704(2) Å c = 7.4250(2) Å α = β = γ = 90°	a = 19.6 Å b = 14.6 Å c = 7.8 Å α = β = γ = 90°
IEZ-FER (calcined)	a = 23.7462(1) Å b = 13.9891(5) Å c = 7.4012(1) Å α = β = γ = 90°	a = 24.2 Å b = 14.4 Å c = 7.6 Å α = β = γ = 90°
difference	4.97	4.6

[a] Unit-cell parameters were calculated by DICVOL program without further refinement. [b] Unit-cell parameters were obtained from ED data without the calibration of camera length.

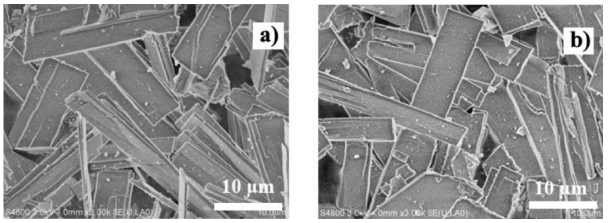

Figure 2. SEM images of calcined (a) 3D FER, and (b) IEZ-FER.

a parameter increased by 4.6 Å, but *b* and *c* parameters almost did not alter, which are in good agreement with the XRD results. The slight difference in the lattice parameters between EM and XRD results is within the error of methods.

During the ED observation, many SAED patterns taken with [010] and [001] incidences were obtained to confirm whether the expansion occurred uniformly or not in the interlayer space. We found that in all crystals, *a* increases in similar value, whereas *b* and *c* remain the same, which suggests that the interlayer space was expanded uniformly. However, diffuse streaks along *a** were also observed in the SAED patterns taken along [0*kl*] (*k*, *l* = integer and $k \neq l = 0$) directions. The extent of the diffuse streaks varied from one crystal to another crystal, which indicates that some IEZ-FER crystals might contain certain disorder in the stacking of the layers. Figure S1 in the Supporting Information shows

three typical examples, from top to bottom, of the extent to which the diffuse streaks increases. In general, most crystals do not show the strong diffuse streaks, which implies that the silylation of $Me_2Si(OEt)_2$ species was quite good.

IEZ-FER crystals were tilted to determine extinction rules and possible space group. Two series of tilted SAED patterns are given in Figure S2 in the Supporting Information. According to the patterns in Figure 3e−h and Figure S2 in the Supporting Information, observable reflections can be summarized as the following conditions {*hkl*: $h + k + l$ = even; 0*kl*: $k + l$ = even; *h*0*l*: $h + l$ = even; *hk*0: $h + k$ = even; *h*00: h = even; 0*k*0: k = even; 00*l*: l = even}. The conditions suggested the possible space groups of *I*222, $I2_12_12_1$, *Imm*2 (*Im*2*m*, *I*2*mm*) and *Immm*. *Immm* is chosen because of the highest symmetry, which is consistent with the space group of FER reported in the IZA database (also confirmed by series tilting (not shown)).

Figure 4 shows HREM images of calcined IEZ-FER taken with the [010] incidence. The corresponding SAED pattern is given in Figure 3f; FD and the simulated image are shown in the inset in Figure 4a. In Figure 4a, we can clearly see the pentasil layer (a set of 5MRs) in the thin edge of the crystal indicated by white arrows. It is identical as the pentasil layer of calcined 3D FER indicated by white arrows in Figure S3 in the Supporting Information, which strongly demonstrated that IEZ-FER keeps FER pentasil layered structure. However, a major different *a* parameter (24.2 Å in Table 1) was obtained. Because the size of the pentasil layer does not alter, we can conclude the pore in the interlayer was enlarged. Moreover, according to the contrast of pore and expansion (4.6 Å) obtained from Table 1, it can be proposed that the pore in the interlayer is similar to 10MR, which differs from 8MR in 3D FER structure. On the other hand, the disorder domain was also observed in the thick area indicated by the white rectangular

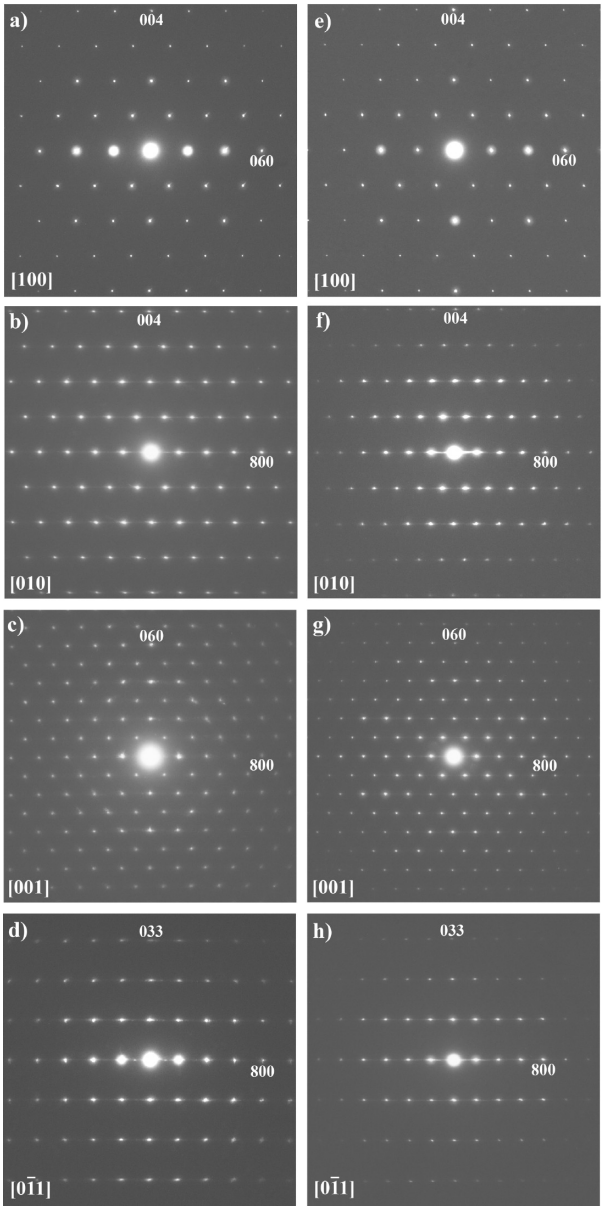

Figure 3. SAED patterns of calcined 3D FER (a−d) and IEZ-FER (e−h) taken along the [100], [010], [001], and [0$\bar{1}$1] directions, respectively.

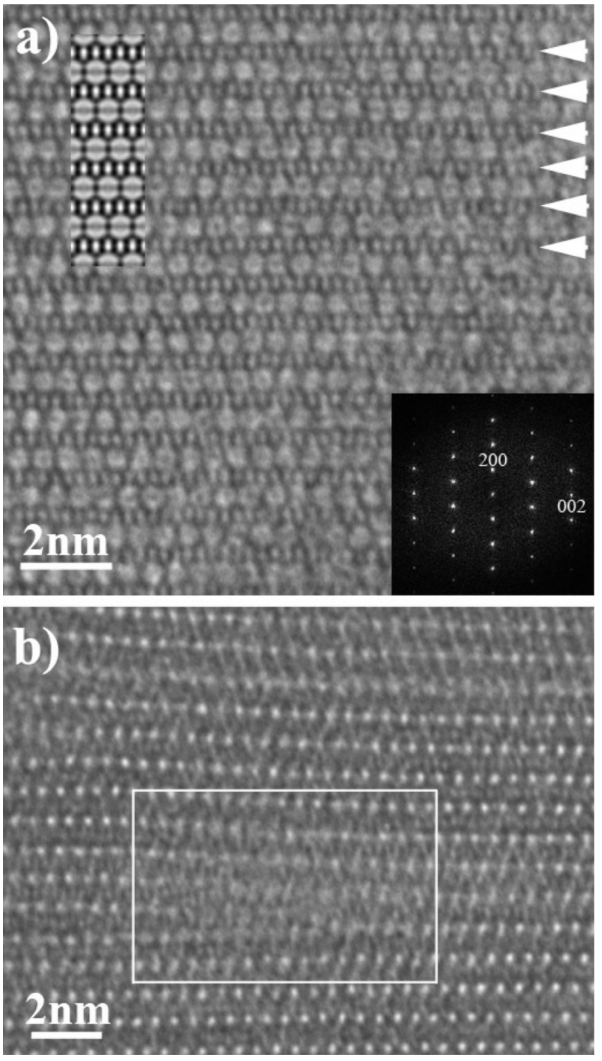

Figure 4. HREM images of (a) thin edge and (b) thick region of calcined IEZ-FER taken along [010] direction. FD and simulated image are inserted in a and pentasil layers are indicated by white arrows. Disordered area is indicated by white rectangular in b.

in Figure 4b. We observed that the layer could collapse or terminate like the formation of dislocation, and then the adjacent layers connected to each other after a certain disordered region, which explains the presence of the diffuse streaks on the SAED pattern.

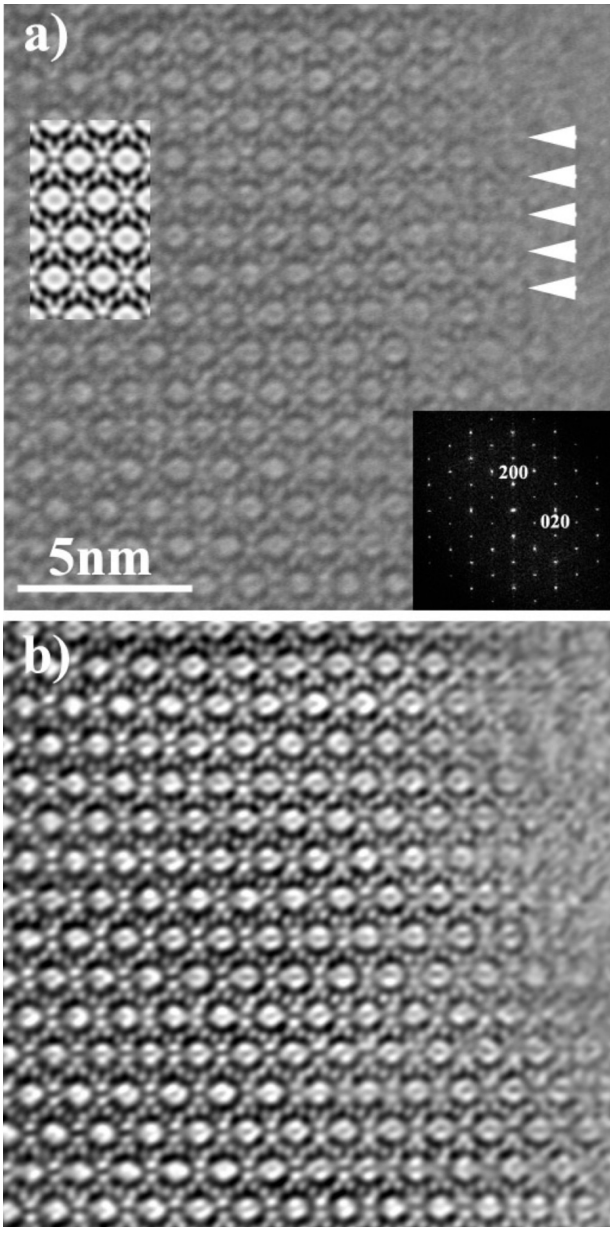

Figure 5. (a) HREM image of calcined IEZ-FER taken along [001] direction with FD and simulated image, and (b) Fourier filtered image of a. Pentasil layers are indicated by white arrows in a.

Figure 5a shows a HREM image of calcined IEZ-FER taken along the [001] direction with the corresponding FD and the simulated image. The corresponding SAED pattern is given in Figure 3g. To enhance the contrast, a Fourier filtered image is given in Figure 5b. In the filtering process, a circular mask was applied to all the Bragg reflections. The image clearly exhibits the pentasil layer indicated by white arrows, which matches the results obtained from the HREM image along the [010] zone axis in Figure 4. Furthermore, we could see 12MR surrounded by twelve 5MRs, which is completely different from 3D FER structure with 10MR surrounded by ten 5MRs. In IEZ-FER, two 5MRs replace 6MR of the 3D FER structure. The presence of 12MR and 10MR in the interlayer space fully verified that the alkoxysilylation method has successfully expanded the interlayer pore window from the precursor PREFER. As a result, 4.97 Å expansion in the interlayer space was achieved due to the silylation.

Figure 6 shows the Ar adsorption/desorption isotherm curves for calcined 3D FER and IEZ-FER. Ar gas adsorption results confirmed the pore of IEZ-FER is indeed larger than that of 3D FER. The pore size distribution shows the average pore size of IEZ-FER is 5.3 Å, which is larger than the average pore size of 3D FER (3.9 Å). In addition, the multipoint Brunauer−Emmett−Teller (BET) surface area for IEZ-FER measured from Ar adsorption was 410 $m^2\ g^{-1}$, which is very similar to that of 3D FER (403 $m^2\ g^{-1}$) because they have the same pentasil layer geometry. The pore volume calculated for IEZ-FER (0.16 mL g^{-1}) was higher than that of 3D FER (0.13 mL g^{-1}) because of the formation of 2D enlarged pore channel system (12MR and 10MR along [001] and [010] directions, respectively) in the interlayer. In comparison to 3D FER, IEZ-FER contains a large quantity of SiOH groups derived from the incorporated $=Si(CH_3)_2$ after burning off the $-CH_3$ groups. The SiOH groups may have a strong interaction with Ar molecules at low temperature like 87 K to make the diffusion of Ar molecules into the inner positions of the channels, which would lead to a delayed uptake of Ar gas on the isotherm of IEZ-FER.

The formation of 12MR and 10MR along the [001] and [010] directions, respectively, can be reasonably

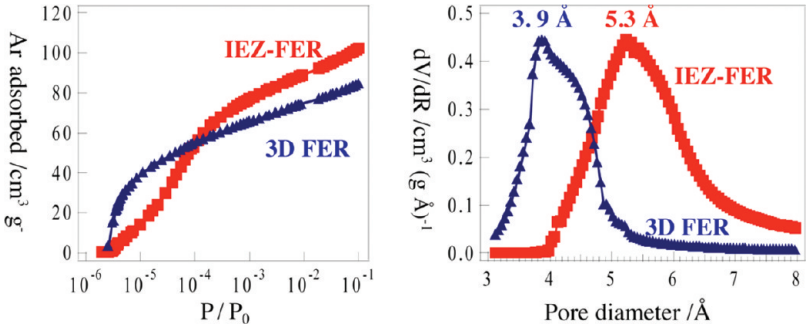

Figure 6. Ar adsorption/desorption isotherm and pore size distribution of calcined 3D FER and IEZ-FER.

illustrated by Scheme 1 and further supported by the ^{29}Si MAS NMR spectrum in Figure 7. PREFER gave the Q^3 and Q^4 bands in the spectrum (Figure 7a). After the alkoxysilylation with $Me_2Si(OEt)_2$, the $Me_2Si(O-)_2$ species were pillared into the interlayer and bonded to pentasil layers through oxygen atoms, which developed a D^2 band and resulted in greatly decreased Q^3 in the spectrum (Figure 7b). However, when the alkoxysilylation is incomplete, the Si atoms on the PREFER layer surface that ideally are expected to connect to pillaring T sites remain as intact Q^3 groups. Upon calcination, methyl groups were replaced by silanol groups, resulting in the $(HO)_2Si(O-)_2$ species which were connected to the adjacent pentasil layers. Because the two pillared T sites are within hydrogen-bonding distance from one another, they readily condense to form adjacent 5MRs. This leads to the absence of D^2 band and a slight increase of the Q^3 band in the spectrum in Figure 7c. Therefore, after calcinations pillared Si atoms exist as a $Si(OH)(SiO_2)_3$ linkage in the interlayer. However, if any pillar T sites are missing, then the nearest neighbor pillared Si atom cannot condense to its vacant neighbor pillar site and hence remains as a $Si(OH)_2(SiO_2)_2$ interlayer linkage, resulting in the presence of Q^2 band in the spectrum in Figure 7c. From Figure 7c, we find that IEZ-FER contains 84.5% Q^4, 13.1% Q^3, and 2.4% Q^2 as given by deconvolution (see Figure S4 in the Supporting Information). If we assume complete silylation with full pillaring, IEZ-FER has 4 pillared Si atoms and 36 Si atoms from the framework per unit cell. Hence, IEZ-FER ideally contains 10% Q^3 groups (neglecting the fraction of Q^3 groups on the external surface of the crystals) and 90% Q^4 groups. If the internal condensation between the pillar sites does not take place, the ratio of Q^4:Q^3:Q^2 would be 90:0:10. However, the presence of 2.4% Q^2 group suggests that the silylation was incomplete; and 2.4% missing pillared Si atoms will cause $2 \times 2.4 = 4.8\%$ Si atoms to be uncoordinated on each PREFER layer giving rise to a Q^3 signal rather than Q^4's. Therefore, on the basis of the Q^2 estimated from Figure 7c, IEZ-FER should contain 85.2% Q^4 and 12.4% Q^3 by calculation, whereas the experiments showed 84.5% Q^4 and 13.1% Q^3. Given the fact that the surface of the crystal will certainly exhibit Q^3 group, possibly Q^2 and a non-negligible concentration of point and extended defects (giving rise to Q^3 nests and isolated silanol groups), the agreement between the idealized ratio of Q^4:Q^3:Q^2 and the measured ratio of Q^4:Q^3:Q^2 is surprisingly good.

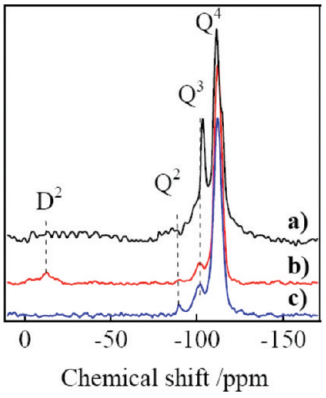

Figure 7. ^{29}Si MAS NMR spectra of (a) PREFER, (b) noncalcined IEZ-FER, and (c) calcined IEZ-FER.

To further probe the nature of the pillared Si atoms, a computational study was instigated. Three distinct geometries for the IEZ-FER in the interlayer space were constructed and relaxed which are shown in Figure 8a–c, which will be referred to as A, B, and C, respectively. The unit-cell parameters for A, B, and C are given in Table S1 in the Supporting Information. Figure 8a shows a supercell of the structure after relaxation. In this structure, the Q^3 sites were initially arranged so that silanol groups (indicated by black arrows) are on opposite sides of the two five rings that connect the pentasil layers.

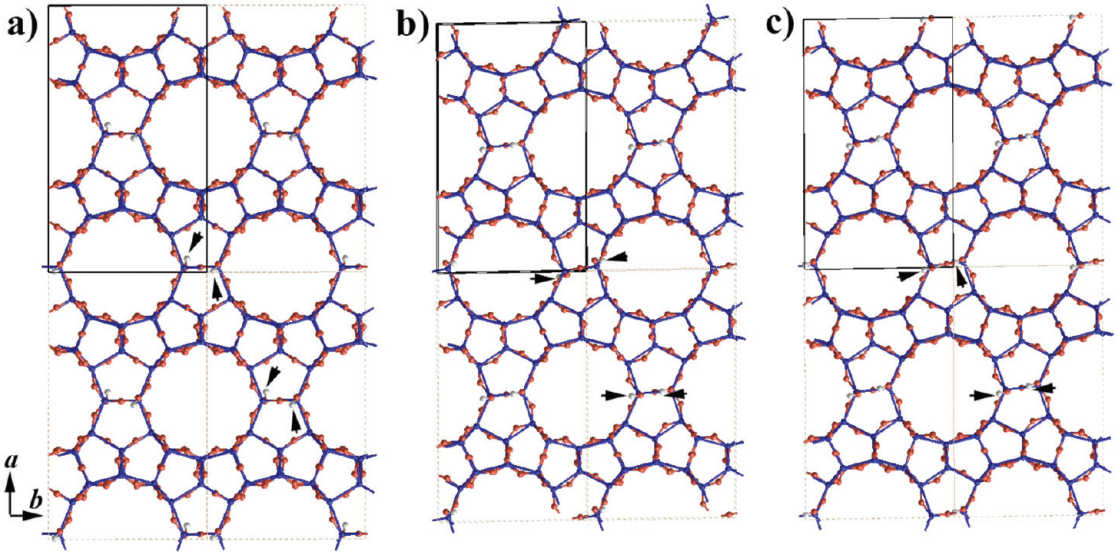

Figure 8. Three distinct geometries of calcined IEZ-FER in the interlayer space: (a) four silanol groups indicated by black arrows sit on opposite sides of the two 5MRs; (b) two silanol groups sit on the same side of the two 5MRs and two silanol groups sit on opposite sides of the two 5MRs; (c) four silanol groups sit on the same side of the two 5MRs. In each structure, four silanol groups are indicated by black arrow.

After relaxation, the relative orientation of the silanol groups is preserved. In fact, there are four silanol groups associated with the two pillar layers per unit cell. In the arrangement shown in structure A, both pillar sites have silanol groups on opposing sides of the five rings. In Figure 8b, the silanol groups (indicated by black arrows) were arranged so that on one pillar site, two silanol groups are on the same side of the two five rings between the pentasil layers, whereas on the other pillar site, the silanol groups are on opposite sides of the five rings. In this arrangement, a weak linear hydrogen bond of length 2.15 Å is formed, measured after relaxation. In the final structure C shown in Figure 8c, all the silanol groups (indicated by black arrows) are on the same side of the five rings and thus two hydrogen bonds are formed per unit cell, with lengths of 2.17 Å. Structure B is most stable, followed by structure C, which is less stable than B by 0.08 eV. Structure A is notably less stable than B, being 0.48 eV higher in energy, and underlines the idea that vacancies in the idealized lattice exist rather than unreacted Q^2, as seen from the NMR data.

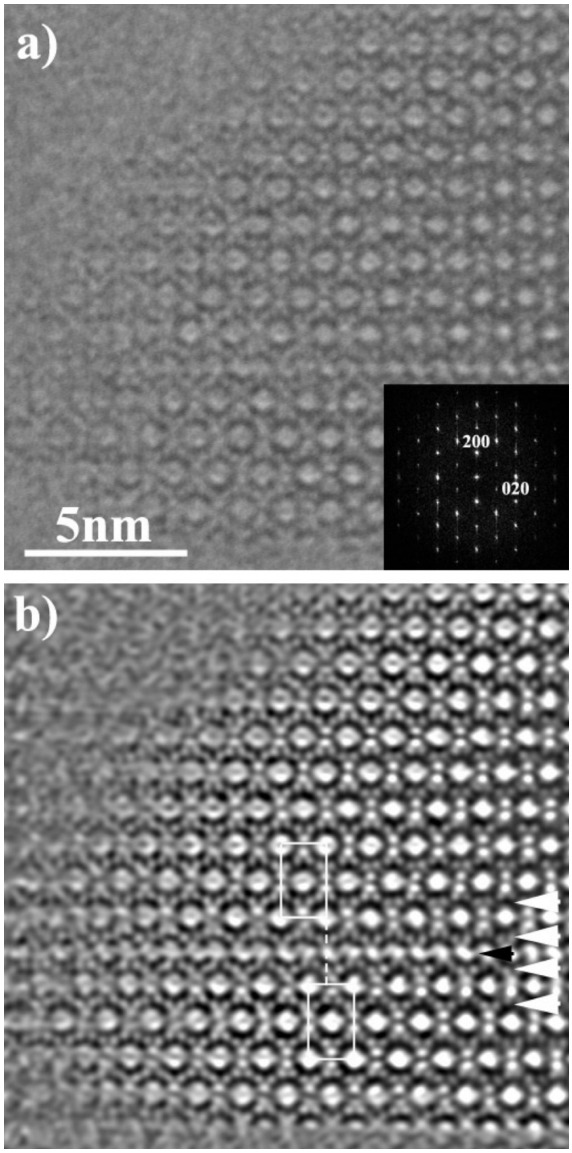

Figure 9. (a) HREM image of calcined IEZ-FER taken along [001] direction with FD, and (b) Fourier filtered image of a. In b, unit cell of IEZ-FER is indicated by white rectangular, and ca. 1/2 *b* shift is indicated by white dashed line. Pentasil layers are indicated by white arrows and disordered area is indicated by black arrow.

The calculations indicate that two structures are probably thermally accessible at room temperature and more elevated temperatures, namely structures B and C. In the case of the minimum energy structure, structure B, the silanol groups are qualitatively different; those that are hydrogen bonded will be relatively static, whereas the silanol groups that are an opposite sides of the pillar face will be more mobile. Specifically, the hydrogen of the silanol group will precess and the tetrahedron cannot invert, so no hydrogen bond is possible with its nearest neighbor silanol group. In structure C, all the silanol groups are hydrogen bonded and thus the silanol group protons will be relatively static. In both structures B and C, there is strain in the structure that manifests itself by the cell angles deforming so that cell becomes triclinic. On an extended length scale, it is speculated that the structure will consist of regions consisting of structure B and bands of structure C, where isolated silanol groups and hydrogen-bonded silanol groups occur in an aperiodic fashion.

Using the structures A, B, and C, HREM images along the [010] and [001] directions were simulated by multislice method. Figure S5 in the Supporting Information show simulated images from three structures with observed images. Comparing the simulated to the observed, the simulated image from three structures all matches the observed image along the [001] zone axis. However, the simulated image from structure A fits the observed images along the [010] zone axis closely than another two structures B and C, even though structure B is the most stable arrangement on enthalpic grounds. Moreover, if we consider the average structure, the most likely structure is B + C, which will on average appear like A. In structure B (and C), the hydrogen bonds cause a distortion in one direction, and it is equally likely that hydrogen bonds are formed in the opposite direction so these distortions will cancel, giving a symmetric pattern similar to A. Therefore, the simulated images from structure A were selected to insert in Figure 5a and 6a for pictorial reasons.

All studies above demonstrate that the expansion of the pore window in the interlayer of IEZ-FER was very successfully obtained, however, during the HREM observations, defects have also been observed which are given in Figures 9 and Figures S6 and S7 in the Supporting Information. Figure 9 shows a disorder structure indicated by black arrow, which can be formed by ca. 1/2 *b* shift of the pentasil layer indicated by white arrows. It is known that framework of CDO is very similar to that of FER. Both structures have a pentasil layer in common, but a stacking period of the layer is different, which is half shift along *b* axis.[5] Therefore, we suggested that the disorder structure may be related to the expanded form of CDO (IEZ-CDO). When two Si atoms were pillared, and the adjacent pentasil layer shifted ca. 1/2 *b*, these two

Si atoms could not condense to each other and just sit alone; it then produces the IEZ-CDO[22] structure with 2D 10MR channel system, not IEZ-FER structure. In Figure S6 in the Supporting Information, we also found the disordered structure (indicated by black arrow) formed by *c*a. 2/7 *b* shift of the pentasil layer indicated by white arrows, which explains the presence of commensurate modulation in Figure S7 of the Supporting Information (indicated by white arrows). Six extra weak spots were observed between the sharp Bragg spots of IEZ-FER in the SAED pattern indicated by two white bars. Moreover, again, a half unit cell shift along the *b* direction indicated by a white dashed line was also observed in Figure S7 of the Supporting Information.

Conclusions

In summary, the new interlayer expanded zeolite IEZ-FER consists of a pentasil layer structure similar to 3D FER with a large increase in the *a* parameter perpendicular to the layer; the expansion of *a* parameter could be explained by the insertion of monomeric Si species and the formation of new Si−O−Si linkages in the interlayer space. The pillaring of the T sites in the interlayer space leads to a new 12MR and 10MR pore channel system along the [001] and [010] directions, respectively. According to our previous and present studies on MWW and FER, we concluded that the modification of layered precursors by alkoxysilylation is a very promising way to obtain new 3D crystalline zeolitic materials with expanded pore window. The interlayer alkoxysilyl groups can act as functional group, which could be utilized as a bridging part to form 3D expanded structure.

(22) Ruan, J. F.; Wu, P.; Slater, B.; Terasaki, O. 2009, unpublished work.

Acknowledgment. This work was supported by the Swedish Science Research Council (VR) and the Japan Science and Technology Agency (JST). The Alice & Knut Wallenberg Foundation is also acknowledged for supporting EM center, Stockholm University. We also acknowledge Dr. Yasuhiro Sakamoto for fruitful discussions. P.W. acknowledges the financial support by NSFC (20673038, 20873043), STCSM (08JC1408700), and 973 Program (2006CB202508). B.S. thanks the EPSRC for computing time on the HPC(x) UK national supercomputer facility.

Note Added after ASAP Publication. There was an error in Figure 3 of the version published ASAP May 19, 2009; the corrected version was published ASAP May 22, 2009.

Supporting Information Available: SAED patterns of calcined IEZ-FER, series of tilted SAED patterns of calcined IEZ-FER, HREM image of calcined 3D FER, deconvolution of ^{29}Si MAS NMR spectrum of calcined IEZ-FER, simulated HREM images of calcined IEZ-FER, unit cell parameters of three geometries, and two HREM images of calcined IEZ-FER shown in Figures S1−S7, respectively (PDF). This material is available free of charge via the Internet at http://pubs.acs.org.